iEnergy
LETTER
https://doi.org/10.23919/IEN.2022.0042

Equilibrium mechanism between dc voltage and ac frequency for ac–dc interlinking converters

Haixu Shi[1,2], Kai Sun[2] ✉, Xiaochao Hou[2], Yunwei Li[3] and Haihao Jiang[1]

ABSTRACT

The equilibrium between dc bus voltage and ac bus frequency (Udc-f equilibrium) is the algorithm core of unified control strategies for ac-dc interlinking converters (ILCs), because the equilibrium implements certain mechanism. However, what the mechanism is has not been explicitly explored, which hinders further studies on unified control. This paper reveals that the state-space model of a Udc-f equilibrium controlled ILC is highly similar to that of a shaft-to-shaft machines system. Hence a detailed mechanism is discovered and named "virtual shaft-to-shaft machine (VSSM)" mechanism. A significant feature of VSSM mechanism is self-synchronization without current sampling or ac voltage sampling.

KEYWORDS

Virtual machine, interlinking converter, unified control, microgrid.

In an ac/dc hybrid microgrid, a grid-forming source (GFS) maintains the voltage of the bus which it directly connects to. An ac-dc interlinking converter (ILC) links a dc bus and an ac bus for mutual power support. GFSs can appear on the dc bus or the ac bus, which leads to multiple operation modes of a hybrid microgrid[1,2]. Referring to Figure 1, in the ac dominant mode, GFSs only exist on the ac bus, and the ILC must maintain the dc bus voltage; in the dc dominant mode, GFSs only exist on the dc bus, and the ILC must maintain the voltage of the ac bus; and in the balanced mode, GFSs exist on both buses, and the ILC transmits some power between the buses to balance the microgrid.

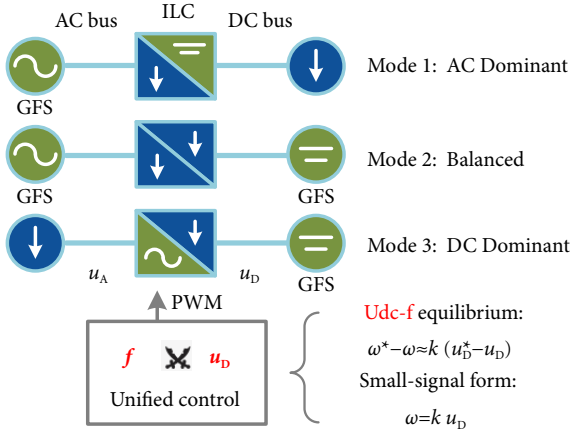

Fig. 1 Unified controls for the ILC in multiple operation modes of a hybrid microgrid.

To adapt to online change of the microgrid-operation mode, one approach is to switch the ILC control loops in line with the changing mode[3,4]. The control-loop switching must keep up with the mode change. Hence, for the ILC, detecting the GFSs' working modes or communicating with the GFSs is always necessary for this case[5], despite efforts to achieve more independently distributed control[6]. To avoid the concern on detection/communication reliability, unified control strategies were developed[7].

$$\omega^* - \omega \approx k\,(u_D^* - u_D) \tag{1}$$

Unified control strategies use a fixed control loop scheme for all operation modes. The equilibrium of dc bus voltage and ac frequency is the core of such control algorithms. This equilibrium is referred to as "Udc-f equilibrium" in this paper and is usually set as Eq. (1) in the literature, where ω is the angular velocity of the ILC modulated voltage, u_D is the dc bus voltage, ω^* and u_D^* are the references of them, and k_1k_1k can be called the matching coefficient[8]. Referring to Eq. (1), the higher u_D is, the higher ω the ILC modulates, and vice versa. Hence, as long as there is a GFS operating on one bus, the voltage stiffness of another bus can be maintained via the ILC.

Droop control is famous for its adaptability, power-sharing ability, and simplicity. An ILC may need to address both the power-dc voltage (P-Udc) droop and the power-frequency (P-f) droop, expressed in Eqs. (2) and (3), which facilitates the establishment of hybrid droop expressed in Eq. (4). P_D and P_A are the expected output powers of the ILC on its dc port and its ac port, respectively.

$$\text{P-Udc droop}: \quad P_D = k_1\,(u_D^* - u_D) \tag{2}$$

$$\text{P-f droop}: \quad P_A = k_2\,(\omega^* - \omega) \tag{3}$$

$$P = P_D - P_A = k_1\,(u_D^* - u_D) - k_2\,(\omega^* - \omega) \tag{4}$$

The hybrid droop is the original form of Udc-f equilibrium[7]. A series of unified control strategies based on Eq. (4) were developed[9–12]. Referring to Eq. (4), pursuing high stiffness of dc

[1]Guangdong Midea Refrigeration Equipment Co., Ltd., Guangdong, Foshan 528311, China; [2]Department of Electrical Engineering, State Key Laboratory of Power Systems, Tsinghua University, Beijing 100084, China; [3]Department of Electrical and Computer Engineering, University of Alberta, Edmonton, AB T6G 1H9, Canada
Address correspondence to Kai Sun, sun-kai@mail.tsinghua.edu.cn

voltage and ac frequency leads to large values of k_1 and k_2, which results in a nearly proportional Udc-f equilibrium as expressed in Eq. (5). Obviously, Eq. (5) has the same form as Eq. (1). And the matching coefficient k in Eq. (1) is k_1/k_2.

$$\text{Large } k_1, k_2: \qquad \omega^* - \omega \approx \frac{k_1}{k_2}\left(u_{\mathrm{D}}^* - u_{\mathrm{D}}\right) \tag{5}$$

By adding regulation loops for the intermediate link voltage, an advanced unified control was developed[8]. Some advanced unified controls were also created by using the virtual synchronous machine technique to set virtual inertia for better dynamic performance[13]. In addition to linear terms of Udc-f equilibrium, quadratic terms were also used to match the order of certain links in system model[10].

The mechanism by Udc-f equilibrium for the entire ILC state-space model has not yet been explored in detail. The mechanism of a basic control approach verifies the reasonability and simplicity of that approach, and it provides setting rules for control parameters. Studies on the mechanisms of phase-lock loop, droop control, and virtual synchronous machine control[14,15] serve as examples. An ac grid system is essentially an inductive rotating inertial system, whereas a dc grid system is essentially a capacitive static inertial system. Udc-f equilibrium is consistent with these inertial natures, and it enabled the development of unified control. A detailed mechanism of the Udc-f equilibrium-controlled ILC should be explored to benefit advanced control studies.

The small-signal form of most Udc-f equilibriums can be derived as Eq. (6), which is also given in Figure 1. The following content of this paper focuses on this small-signal form.

$$\omega = k\,u_{\mathrm{D}} \tag{6}$$

The main contributions of this paper are listed as follows: (1) This paper reveals that the state-space model of a Udc-f equilibrium controlled ILC is highly similar to that of a shaft-to-shaft machines system. Hence a detailed mechanism is discovered and named "virtual shaft-to-shaft machine (VSSM)" mechanism. (2) It is discovered that VSSM mechanism features self-synchronization without current sampling or ac voltage sampling.

1 Udc-f equilibrium controlled ILC and shaft-to-shaft machines

Together, a synchronous machine and a dc machine with a shaft-to-shaft connection can be used as an ac-dc conversion device. A modeling comparison between such a shaft-to-shaft machine system and a three-phase two-level ac-dc ILC is presented to reveal their potential high similarity, as shown in Figure 2. The derivation and explanation for Figure 2 are as follows. The symbol definitions are listed in Table 1. The variables in the ILC are defined using the meaning of state-space averaging. All of the circuit components are assumed to be ideal for simplified analysis.

1.1 Comparison on the ac side

θ is the angle in the abc coordinate system, and ω is its velocity:

$$\theta = \int_{t0}^{t} \omega\,\mathrm{d}t + \theta_0 \tag{7}$$

(1) ILC model

For the ILC, referring to Figure 2, the state equation on the ac side is shown in Eq. (8):

Table 1 Symbol definition of ILC and shaft-to-shaft machines

Symbol	Object
u_{abc}, u_{dq0}	ac bus voltages; as in the dq axis
i_{abc}, i_{dq0}	ac port currents; as in the dq axis
L	filter inductor; machine leakage inductance
ψ_{abc}, ψ_{dq0}	ac filter inductor fluxes; as in the dq axis
r	Inductor parasitic resistance
e_{abc}, e_{dq0}	Modulated voltages; as in the dq axis
C_{D}	dc bus capacitor
u_{D}, e_{D}	dc port voltage, dc machine electromotive force
ψ_{A}	Synchronous machine air gap coupled flux
ψ_{D}	dc machine transferred air gap coupled flux
ψ_{mabc}, ψ_{mdq0}	Synchronous machine flux; as in the dq axis
e_{mabc}, e_{mdq0}	Synchronous machine electromotive force in dq axis
J	Total moment of inertia including shafts and rotors

$$\begin{bmatrix} u_a \\ u_b \\ u_c \end{bmatrix} = \frac{\mathrm{d}}{\mathrm{d}t}\begin{bmatrix} \psi_a \\ \psi_b \\ \psi_c \end{bmatrix} + \begin{bmatrix} ri_a \\ ri_b \\ ri_c \end{bmatrix} + \begin{bmatrix} e_a \\ e_b \\ e_c \end{bmatrix} \tag{8}$$

Eq. (8) can be transformed into the dq coordinate system, as shown in Eq. (9):

$$\begin{bmatrix} u_d \\ u_q \\ u_0 \end{bmatrix} = \begin{bmatrix} 0 & -\omega & 0 \\ \omega & 0 & 0 \\ 0 & 0 & 0 \end{bmatrix}\begin{bmatrix} \psi_d \\ \psi_q \\ \psi_0 \end{bmatrix} + \frac{\mathrm{d}}{\mathrm{d}t}\begin{bmatrix} \psi_d \\ \psi_q \\ \psi_0 \end{bmatrix} + r\begin{bmatrix} i_d \\ i_q \\ i_0 \end{bmatrix} + \begin{bmatrix} e_d \\ e_q \\ e_0 \end{bmatrix} \tag{9}$$

where

$$\begin{bmatrix} \psi_d \\ \psi_q \\ \psi_0 \end{bmatrix} = \begin{bmatrix} L & 0 & 0 \\ 0 & L & 0 \\ 0 & 0 & L \end{bmatrix}\begin{bmatrix} i_d \\ i_q \\ i_0 \end{bmatrix}.$$

Then Eq. (9) can be simplified as Eq. (10) with the remaining dq quantities:

$$\begin{bmatrix} u_d \\ u_q \end{bmatrix} = \begin{bmatrix} -\omega L i_q + L\dfrac{\mathrm{d}i_d}{\mathrm{d}t} + ri_d + e_d \\ \omega L i_d + L\dfrac{\mathrm{d}i_q}{\mathrm{d}t} + ri_q + e_q \end{bmatrix} \tag{10}$$

(2) Shaft-to-shaft machines model

For the shaft-to-shaft machines, referring to Figure 2, the state equation for the ac armature is as shown in Eq. (11):

$$\begin{bmatrix} u_a \\ u_b \\ u_c \end{bmatrix} = \frac{\mathrm{d}}{\mathrm{d}t}\begin{bmatrix} \psi_{\mathrm{ma}} \\ \psi_{\mathrm{mb}} \\ \psi_{\mathrm{mc}} \end{bmatrix} + \begin{bmatrix} ri_a \\ ri_b \\ ri_c \end{bmatrix} \tag{11}$$

Eq. (11) can be transformed into the dq coordinate system, as shown in Eq. (12):

$$\begin{bmatrix} u_d \\ u_q \\ u_0 \end{bmatrix} = \begin{bmatrix} 0 & -\omega & 0 \\ \omega & 0 & 0 \\ 0 & 0 & 0 \end{bmatrix}\begin{bmatrix} \psi_{md} \\ \psi_{mq} \\ \psi_{\mathrm{m0}} \end{bmatrix} + \frac{\mathrm{d}}{\mathrm{d}t}\begin{bmatrix} \psi_{md} \\ \psi_{mq} \\ \psi_{\mathrm{m0}} \end{bmatrix} + r\begin{bmatrix} i_d \\ i_q \\ i_0 \end{bmatrix} \tag{12}$$

The synchronous machine is assumed to be ideal. Non-ideal parameters, like rotor damping windings and the armature reaction, can be neglected[16]. Thus, the flux equation is derived as Eq. (13), where ψ_{A} is the air-gap coupled flux:

$$\begin{bmatrix} \psi_{md} \\ \psi_{mq} \\ \psi_{m0} \end{bmatrix} = \begin{bmatrix} L & 0 & 0 \\ 0 & L & 0 \\ 0 & 0 & L \end{bmatrix} \begin{bmatrix} i_d \\ i_q \\ i_0 \end{bmatrix} + \begin{bmatrix} \psi_A \\ 0 \\ 0 \end{bmatrix} \tag{13}$$

Then the state equation (12) is simplified as shown in Eq. (14), where e_{md} and e_{mq} represent the electromotive force:

$$\begin{bmatrix} u_d \\ u_q \end{bmatrix} = \begin{bmatrix} -\omega L i_q + L\dfrac{\mathrm{d}i_d}{\mathrm{d}t} + ri_d + \underbrace{0}_{e_{md}} \\ \omega L i_d + L\dfrac{\mathrm{d}i_q}{\mathrm{d}t} + ri_q + \underbrace{\omega\psi_A}_{e_{mq}} \end{bmatrix} \tag{14}$$

For ac part, obviously, the state equations of the ILC and the synchronous machine, namely Eqs. (10) and (14), are equivalent as long as the ILC modulates the fundamental voltage equal to the electromotive force of the synchronous machine, as shown in Eq. (15):

$$\begin{cases} e_d = e_{md} = 0 \\ e_q = e_{mq} = \omega\psi_A \end{cases} \tag{15}$$

1.2 Comparison on the dc side and the inertia link

The inertia state equation of the dc capacitor in the ILC is easily derived as shown in Eq. (16):

$$C_D u_D \frac{\mathrm{d}u_D}{\mathrm{d}t} = P_{AC} - P_{DC} = \frac{3}{2}(e_d i_d + e_q i_q) - P_{DC} \tag{16}$$

The inertia state equation of the rotor (or shaft) angular velocity in the shaft-to-shaft machine is easily derived as shown in Eq. (17). Obviously, if the ILC control ensures a proportion between u_D and ω, the inertia equations (16) and (17) have the same form.

$$J\omega\frac{\mathrm{d}\omega}{\mathrm{d}t} = P_{AC} - P_{DC} = \frac{3}{2}(e_{md} i_d + e_{mq} i_q) - P_{DC} \tag{17}$$

For an ideal dc machine, the relationship between the dc port voltage u_D, the dc electromotive force e_D and the rotor angular velocity is given as Eq. (18), where ψ_D is the transferred air-gap coupled flux of the dc machine:

$$u_D = e_D = \omega\ \psi_D \tag{18}$$

Eq. (18) is exactly the proportional relationship needed for ILC control to make Eqs. (16) and (17) equivalent. And Eq. (18) is also exactly the small-signal Udc-f equilibrium expressed in Eq. (6). Combining Eqs. (16)–(18), Eq. (19) can be derived.

$$J = C_D\psi_D^2 = C_D / k^2 \tag{19}$$

Eq. (19) reveals that the moment of inertia in the shaft-to-shaft machine system can be physically and linearly emulated by the dc bus capacitance of an ILC.

1.3 Equivalence condition and the VSSM mechanism

Combining Eqs. (15) and (18), Eq. (20) is obtained as the full condition to make the ILC state-space model (i.e., Eqs. (10) and (16)) strictly equivalent to the shaft-to-shaft machine system state-space model (i.e., Eqs. (14), (17), and (18)), where $k = 1/\Psi_D$, $M = \Psi_A/\Psi_D$. For better readability, the derivation of model equivalence is summarized in Figure 2.

$$\{\omega = k u_D, \quad e_d = 0, \quad e_q = M u_D \tag{20}$$

The model equivalence, as shown in Figure 2, means that the Udc-f equilibrium controlled ILC copies the mechanism of the shaft-to-shaft machines in terms of port characteristic. Hence the mechanism in such an ILC is named "virtual shaft-to-shaft machine (VSSM)" mechanism. As shown in Figure 3, the control loop for Eq. (20) implements the VSSM mechanism. This VSSM loop contains the Udc-f equilibrium Eq. (6). Referring to Figure 3, there is no current sampling or ac voltage sampling. This is a great simplicity for realization of the VSSM mechanism.

2 Self-synchronization of Udc-f equilibrium

The Udc-f equilibrium controlled ILC features self-synchronization due to the VSSM mechanism. In control studies using the definition of Udc-f equilibrium expressed in Eq. (4), the inner P-f droop was considered as the reason for self-synchronization. The P-f droop requires current sampling. However, for the VSSM mechanism, there is no current sampling or ac voltage sampling, so the P-f droop self-synchronization principle does Eq. not apply to it.

The system transmission diagram of the VSSM loop controlled

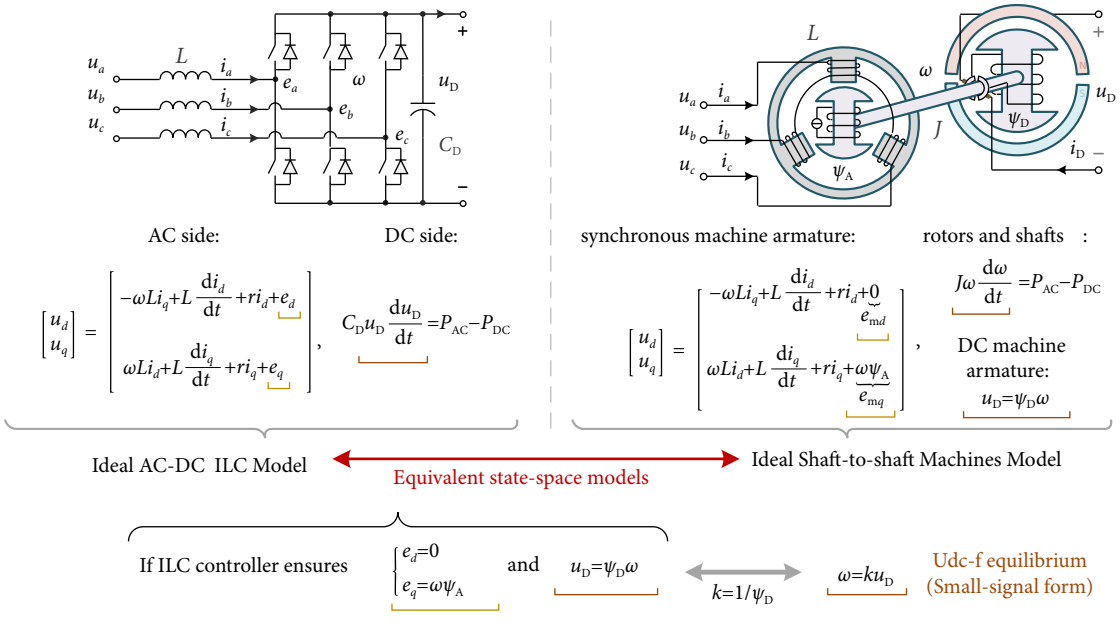

Fig. 2 Model comparison between an ac-dc ILC and a shaft-to-shaft machine system.

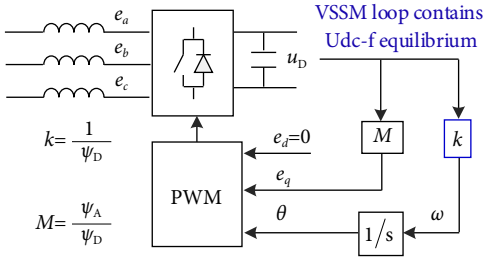

Fig. 3 The VSSM loop contains Udc-f equilibrium.

ILC is presented as Figure 4, including the power circuit part and the controller part. A transmission link from u_D to ω is necessary to form a negative feedback loop for the regulation of the phase difference $\theta_g - \theta$. The Udc-f equilibrium Eq. (6) is such a simple link. Hence, $\theta_g - \theta$ can be adaptively regulated to a certain value in steady state, which means the self-synchronization is achieved, just as the self-synchronization in the shaft-to-shaft machines.

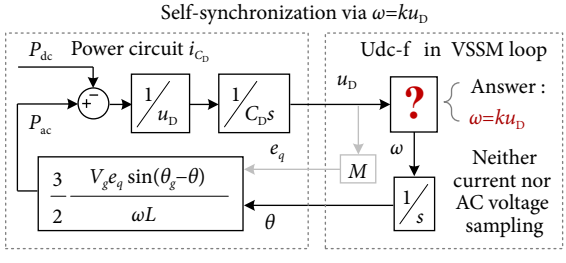

Fig. 4 Self-synchronization principle of the VSSM mechanism.

A simple but typical microgrid configuration is selected as shown in Figure 5. For the ac GFS, the voltage amplitude is V_g and the angular velocity is ω_g. The dc GFS is under a droop control, where V_D is its dc voltage reference and r_D is its droop coefficient. The ILC links both buses. The loads are resistors R_A and R_D. C is the ac filter capacitance. A detailed switching-model simulation in Simulink/MATLAB is established to provide a set of time-domain waveforms to help illustrate the self-synchronization principle. The microgrid-operation modes shown in Figure 1 are determined by the states of the contactors S_A and S_D shown in Figure 5. The main parameters are listed in Table 2.

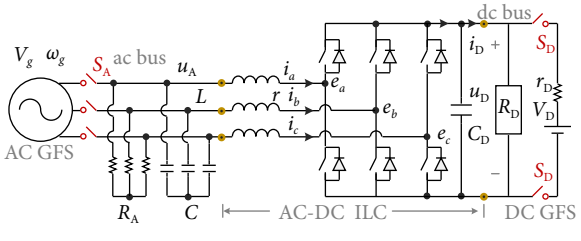

Fig. 5 A detailed configuration of a hybrid microgrid.

The simulation results are shown in Figure 6. In the ac dominant mode, S_A is on and S_D is off, and a transient process of load R_D stepping from 20 to 40 Ω is recorded.

The negative-feedback regulation of $\theta_g - \theta$ via u_D can be observed. In Figure 6(a), the load shed causes u_D to increase at the beginning. The Udc-f equilibrium Eq. (6) makes ω increase at the same time, leading to a drop of $\theta_g - \theta$. When the drop of $\theta_g - \theta$ causes the active power to be lower than the dc load consumption, u_D begins to decrease. Due to the integral link, $\theta_g - \theta$ has a 90° delay compared to u_D. After the oscillation, u_D returns to its initial steady-state value, whereas $\theta_g - \theta$ reaches a new steady state value to match the power consumption change. This verifies the self-synchronization of the VSSM mechanism. Figure 6(b) presents the self-synchronization process in the form of phase plane, which helps understand the regulation relationship between $\theta_g - \theta$ and u_D. The constant steady-state u_D value verifies that u_D is maintained via the proportion between u_D and ω_g.

Table 2 System parameters for the microgrid

Symbol	Value	Symbol	Value
rated V_g	110 V rms	L	1.0 mH
rated ω_g,ω	60 × 2π rad/s	r	0.050 Ω
rated V_D	380 V dc	U_A rated	110 V rms
r_D	6.0 Ω	u_D rated	380 V dc
C_D	130 μF	f_{PWM}	100 kHz
C	3.3 μF	Ψ_A	rated $\sqrt{2}U_A/\omega$
rated power	2.0 kW	Ψ_D	rated u_D/ω

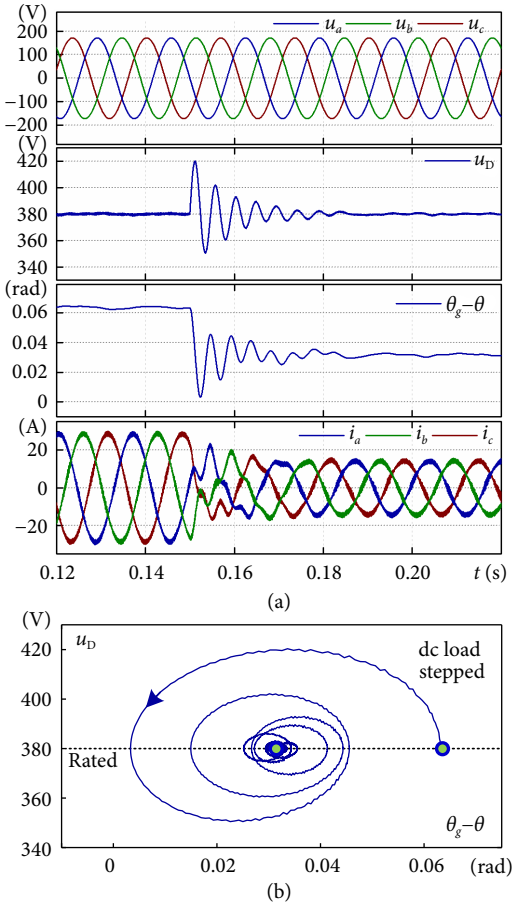

Fig. 6 The self-synchronization of the VSSM mechanism in load step response: (a) waveform in time domain, (b) plane domain.

3 Experiment

A 2 kW/60 Hz 110 VAC/380 VDC hybrid microgrid prototype using MOSFET (model number C3M0075120J) was built to conduct an experimental verification. The configuration of the microgrid is the same as shown in Figure 5. The system parameters are the same as in Table 2.

3.1 Multi-mode adaption

The prototype initially operates in the balanced mode. The ILC is controlled with the VSSM loop as shown in Figure 3. The ac grid frequency value is fixed. Hence, the steady-state value of u_D is clamped by the frequency. The dc GFS then determines its power via its droop control. And the ILC transmits this power to balance both buses. Figure 7 shows a switching process to the dc dominant mode, and Figure 8 shows a switching process to the ac dominant mode. The AB-line voltage of the ac GFS is referred to as u_{gab}, that of the local ac bus is referred to as u_{ab}, and the current of the phase-A is referred to as i_a.

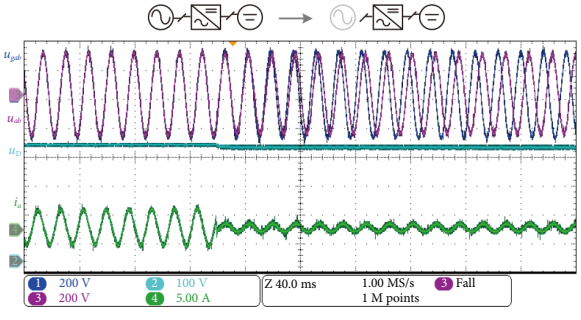

Fig. 7 Switching process from the balanced mode to the dc dominant mode with the VSSM loop.

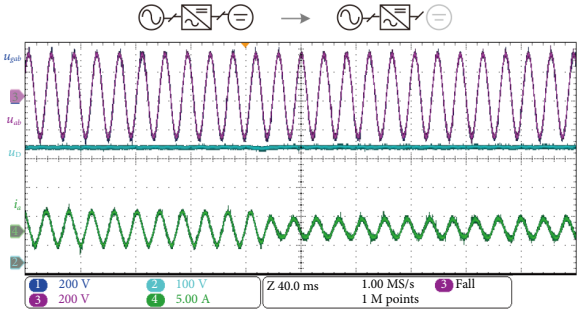

Fig. 8 Switching process from the balanced mode to the ac dominant mode with the VSSM loop.

Referring to Figure 7, when the ac electromagnetic connector S_A is switched off, the ac local voltage becomes independent from the ac grid voltage. The dc bus voltage u_D is still maintained by the dc GFS, whereas the ac phase voltage amplitude U_A and its frequency ω are maintained via the Udc-f equilibrium (6) and the modulation index Eq. (20). The transient process is short and smooth.

Referring to Figure 8, when the dc GFS is disconnected from the dc bus, the steady-state value of u_D is still clamped by the ac grid frequency via the Udc-f equilibrium Eq. (6). The transient process is also short and smooth.

The mode switching tests shown in Figures 7 and 8 verify that the Udc-f equilibrium Eq. (6) is the algorithm core of unified control strategies for ILC due to the VSSM mechanism.

3.2 Self-synchronization on ac side

Figure 9 shows a load step test in the ac dominant mode, where no dc GFS maintains u_D. The ILC is controlled with the VSSM loop as shown in Figure 3. When the load R_D steps from 300 to 120 Ω, a transient process is triggered. After the oscillation, u_D returns to its initial steady-state value (the rated value). The ILC regulates its power to match the new load consumption. The

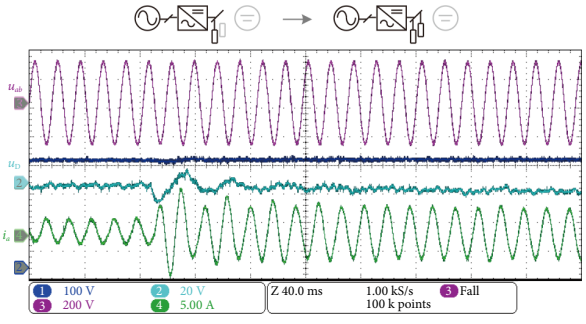

Fig. 9 Load step response in the ac dominant mode with Udc-f equilibrium.

power increase and the synchronization are indicated by the i_a waveform. The simulation in Figure 6 was verified.

4 Conclusions

Udc-f equilibrium is the algorithm core of unified control strategies for ac-dc ILCs, because the equilibrium implements certain mechanism. However, what the mechanism is has not been explicitly explored, which hinders further studies on unified control. This paper reveals that an ILC under unified control is highly similar to a shaft-to-shaft machine system in the sense of full-order state-space modeling, due to the Udc-f equilibrium. Hence a detailed mechanism is discovered and named "virtual shaft-to-shaft machine (VSSM)" mechanism. It is also verified that even the VSSM mechanism features self-synchronization. This self-synchronization principle is similar to that of the shaft-to-shaft machine system, and it is different from P-f droop since there is no current sampling. The VSSM mechanism does not need ac voltage sampling either.

Acknowledgment

This work was supported in part by the National Natural Science Foundation of China under Grants 51877117 and 52007096, the International Joint Mission On Climate Change and Carbon Neutrality, and the Major Science and Technology Innovation Project of Jiangsu Province of China under Grant BE2022038.

Article history

Received: 16 September 2022; Accepted: 2 October 2022

Additional information

Declaration of competing interest

The authors have no competing interests to declare that are relevant to the content of this article.

References

[1] Matic-Cuka, B., Kezunovic, M. (2014). Islanding detection for inverter-based distributed generation using support vector machine method. *IEEE Transactions on Smart Grid*, 5: 2676–2686.

[2] Ma, Y. W., Wang, J. X., Wang, F., Tolbert, L. M. (2018). Converter-based reconfigurable real-time electrical system emulation platform. *Chinese Journal of Electrical Engineering*, 4: 20–27.

[3] Liu, H. P., Loh, P. C., Wang, X. F., Yang, Y. H., Wang, W., Xu, D. G. (2016). Droop control with improved disturbance adaption for a PV system with two power conversion stages. *IEEE Transactions on Industrial Electronics*, 63: 6073–6085.

[4] Yi, Z. H., Dong, W. X., Etemadi, A. H. (2018). A unified control and power management scheme for PV-battery-based hybrid microgrids for both grid-connected and islanded modes. *IEEE Transactions on Smart Grid*, 9: 5975–5985.

[5] Qiu, Z. X., Sun, K. (2017). A photovoltaic generation system based on wide voltage-gain DC-DC converter and differential power processors for DC microgrids. *Chinese Journal of Electrical Engineering*, 3: 84–95.

[6] Guerrero, J. M., Chandorkar, M., Lee, T. L., Loh, P. C. (2013). Advanced control architectures for intelligent microgrids —Part I: Decentralized and hierarchical control. *IEEE Transactions on Industrial Electronics*, 60: 1254–1262.

[7] Loh, P. C., Li, D., Chai, Y. K., Blaabjerg, F. (2013). Autonomous operation of hybrid microgrid with AC and DC subgrids. *IEEE Transactions on Power Electronics*, 28: 2214–2223.

[8] Gu, Y. J., Li, Y. T., Yoo, H. J., Nguyen, T. T., Xiang, X., Kim, H. M., Junyent-Ferre, A., Green, T. C. (2019). Transfverter: Imbuing transformer-like properties in an interlink converter for robust control of a hybrid AC–DC microgrid. *IEEE Transactions on Power Electronics*, 34: 11332–11341.

[9] Ji, Y., Wu, M., Liu, H. T., Li, Y., Zhang, Y. (2016). Bidirectional droop control of interlinking converter in AC/DC hybrid micro-grid. In: Proceedings of the 2016 3rd International Conference on Information Science and Control Engineering (ICISCE), Beijing, China.

[10] Cao, Y. J., Wang, W. Y., Li, Y., Tan, Y., Chen, C., He, L., Häger, U., Rehtanz, C. (2018). A virtual synchronous generator control strategy for VSC–MTDC systems. *IEEE Transactions on Energy Conversion*, 33: 750–761.

[11] Wang, J. J., Jin, C., Wang, P. (2018). A uniform control strategy for the interlinking converter in hierarchical controlled hybrid AC/DC microgrids. *IEEE Transactions on Industrial Electronics*, 65: 6188–6197.

[12] Li, X. L., Guo, L., Li, Y. W., Guo, Z., Hong, C., Zhang, Y., Wang, C. S. (2018). A unified control for the DC–AC interlinking converters in hybrid AC/DC microgrids. *IEEE Transactions on Smart Grid*, 9: 6540–6553.

[13] Qi, G. X., Chen, A. L., Chen, J. (2017). Improved control strategy of interlinking converters with synchronous generator characteristic in islanded hybrid AC/DC microgrid. *CPSS Transactions on Power Electronics and Applications*, 2: 149–158.

[14] D'Arco, S., Suul, J. A. (2014). Equivalence of virtual synchronous machines and frequency-droops for converter-based MicroGrids. *IEEE Transactions on Smart Grid*, 5: 394–395.

[15] Zhong, Q. C., Boroyevich, D. (2016). Structural resemblance between droop controllers and phase-locked loops. *IEEE Access*, 4: 5733–5741.

[16] Zhong, Q. C., Weiss, G. (2011). Synchronverters: inverters that mimic synchronous generators. *IEEE Transactions on Industrial Electronics*, 58: 1259–1267.